Catalytic Transformation of Levulinic Acid to 2-Methyltetrahydrofuran Using Ruthenium–N-triphos Complexes Supporting Information

Andreas Phanopoulos, Andrew J. P. White, Nicholas J. Long, Philip W. Miller**

Department of Chemistry, Imperial College London, South Kensington, London, SW7 2AZ, UK.

*email: n.long@imperial.ac.uk (NJL), philip.miller@imperial.ac.uk (PWM)

Gas chromatography traces of representative catalytic runs

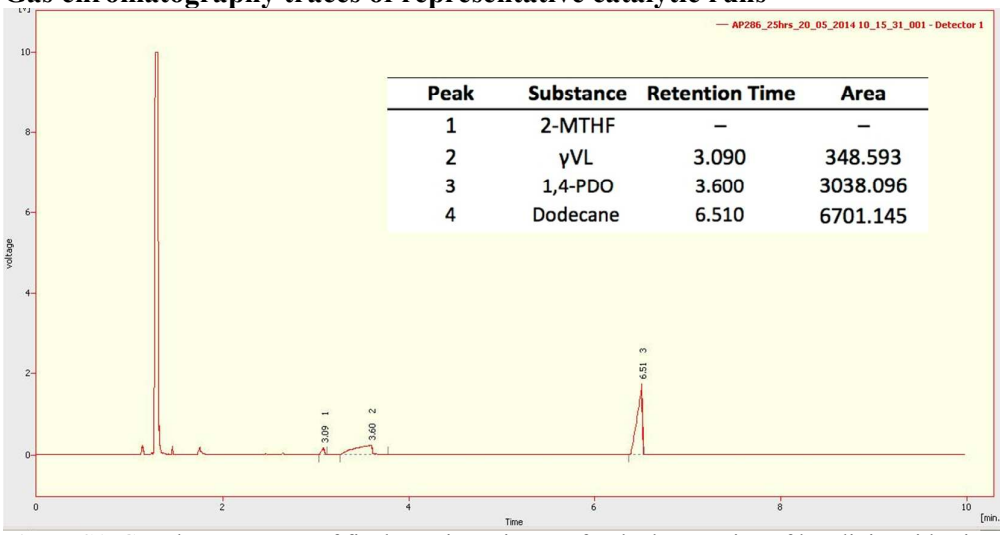

Figure S1. Gas chromatogram of final reaction mixture after hydrogenation of levulinic acid using Triphos^{Ph}/[Ru(acac)$_3$] to generate the catalyst *in situ*. The stated areas were corrected using K_F values determined by calibration experiments with pure substance mixtures.

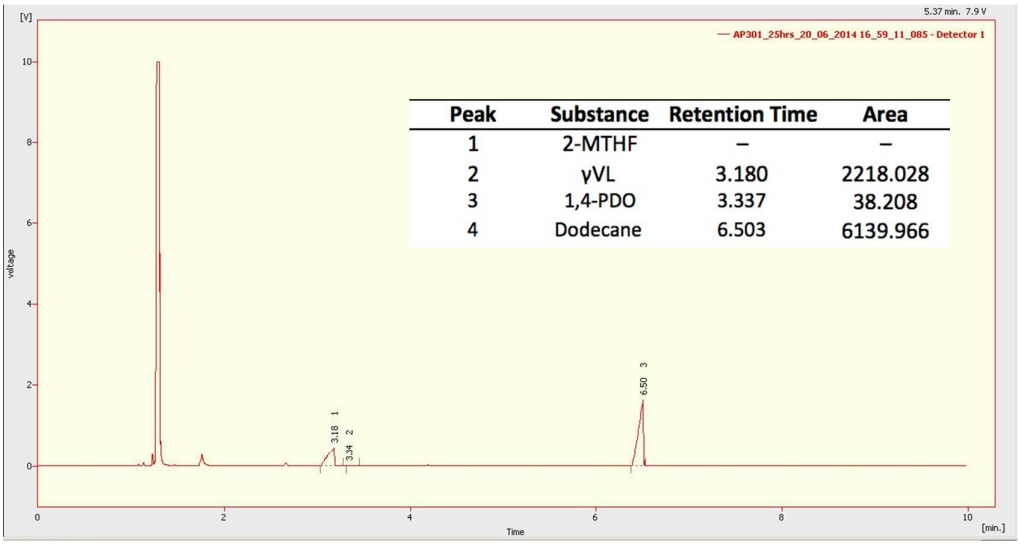

Figure S2. Gas chromatogram of final reaction mixture after hydrogenation of levulinic acid using $[RuH_2(CO)\{CH_3C(CH_2PPh_2)_3\text{-}\kappa^3P\}]$ (**3**) as pre-catalyst. The stated areas were corrected using K_F values determined by calibration experiments with pure substance mixtures.

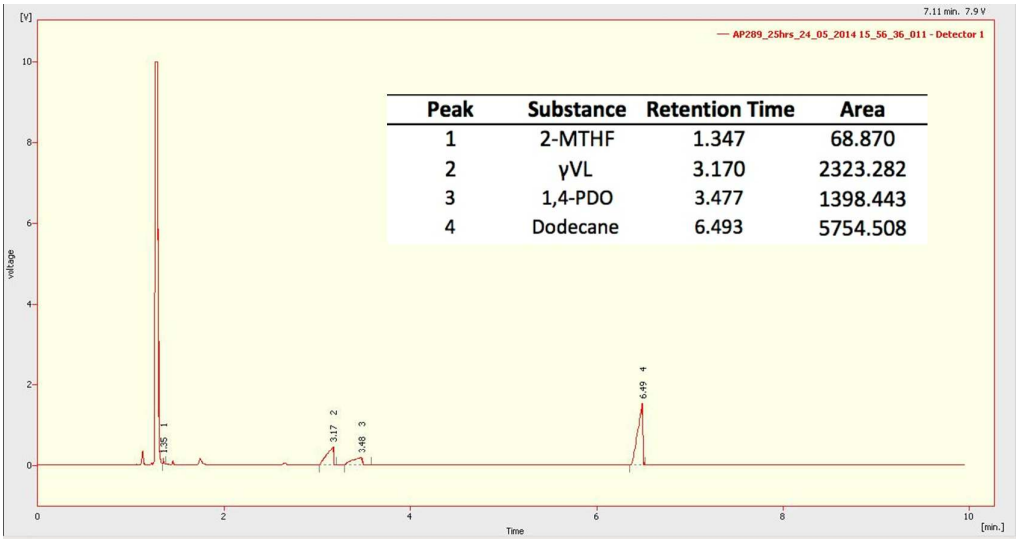

Peak	Substance	Retention Time	Area
1	2-MTHF	1.347	68.870
2	γVL	3.170	2323.282
3	1,4-PDO	3.477	1398.443
4	Dodecane	6.493	5754.508

Figure S3. Gas chromatogram of final reaction mixture after hydrogenation of levulinic acid using N-triphos^{Ph}/$[Ru(acac)_3]$ to generate the catalyst *in situ*. The stated areas were corrected using K_F values determined by calibration experiments with pure substance mixtures.

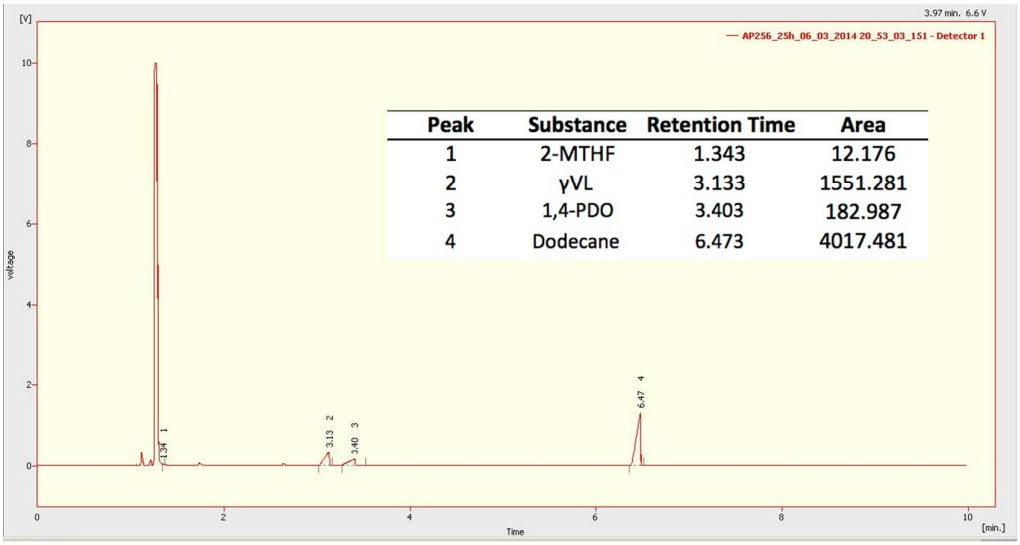

Peak	Substance	Retention Time	Area
1	2-MTHF	1.343	12.176
2	γVL	3.133	1551.281
3	1,4-PDO	3.403	182.987
4	Dodecane	6.473	4017.481

Figure S4. Gas chromatogram of final reaction mixture after hydrogenation of levulinic acid using $[RuH_2(CO)\{N(CH_2PPh_2)_3\text{-}\kappa^3P\}]$ (**4**) as pre-catalyst. The stated areas were corrected using K_F values determined by calibration experiments with pure substance mixtures.

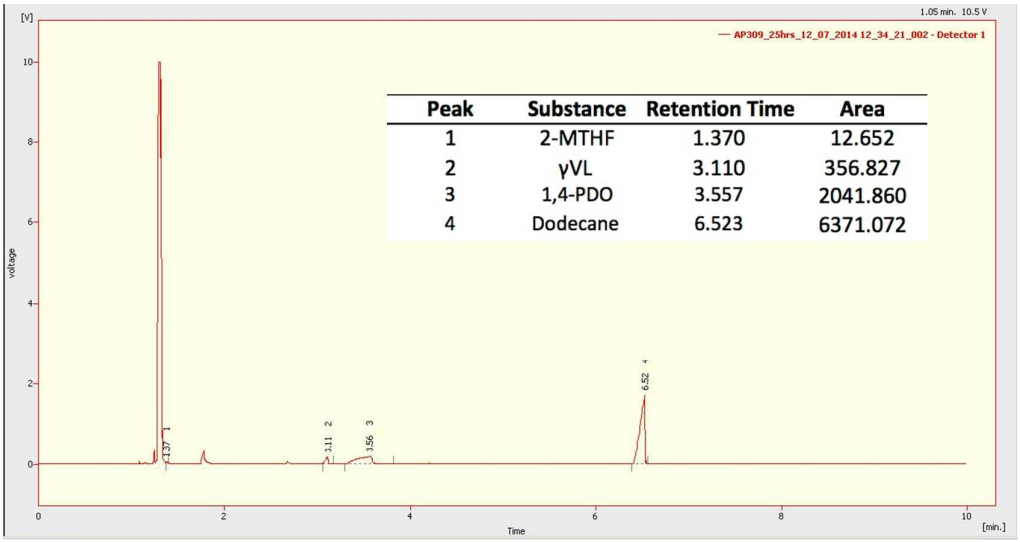

Peak	Substance	Retention Time	Area
1	2-MTHF	1.370	12.652
2	γVL	3.110	356.827
3	1,4-PDO	3.557	2041.860
4	Dodecane	6.523	6371.072

Figure S5. Gas chromatogram of final reaction mixture after hydrogenation of levulinic acid using $[RuH_2(PPh_3)\{N(CH_2PPh_2)_3\text{-}\kappa^3P\}]$ (**5**) as pre-catalyst. The stated areas were corrected using K_F values determined by calibration experiments with pure substance mixtures.

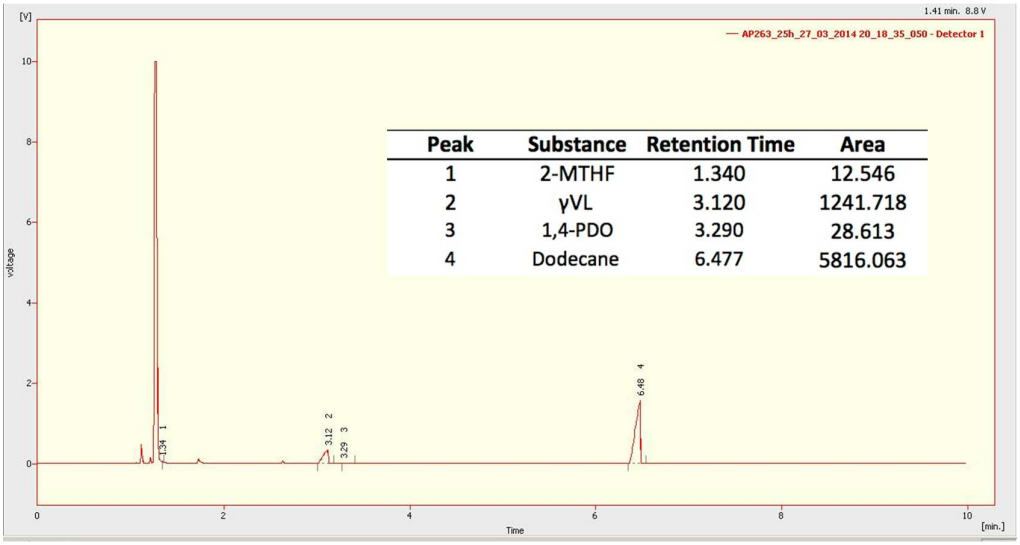

Peak	Substance	Retention Time	Area
1	2-MTHF	1.340	12.546
2	γVL	3.120	1241.718
3	1,4-PDO	3.290	28.613
4	Dodecane	6.477	5816.063

Figure S6. Gas chromatogram of final reaction mixture after hydrogenation of levulinic acid using $[RuH_2(PPh_3)\{N(CH_2PCyp_2)_3\text{-}\kappa^3P\}]$ (**6**) as pre-catalyst. The stated areas were corrected using K_F values determined by calibration experiments with pure substance mixtures.

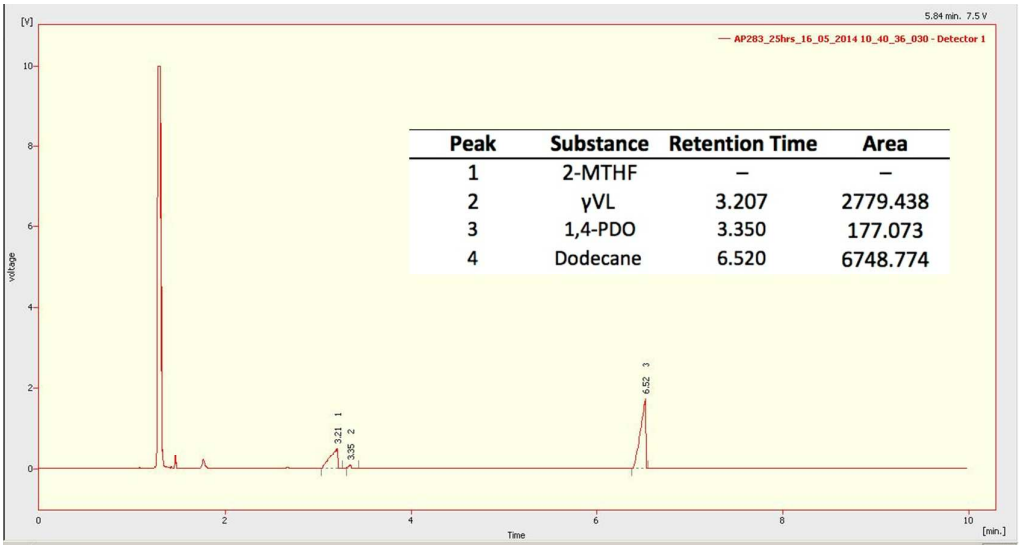

Peak	Substance	Retention Time	Area
1	2-MTHF	–	–
2	γVL	3.207	2779.438
3	1,4-PDO	3.350	177.073
4	Dodecane	6.520	6748.774

Figure S7. Gas chromatogram of final reaction mixture after hydrogenation of levulinic acid using $Triphos^{Ph}$/[$Ru(acac)_3$] and NH_4PF_6 to generate the catalyst *in situ*. The stated areas were corrected using K_F values determined by calibration experiments with pure substance mixtures.

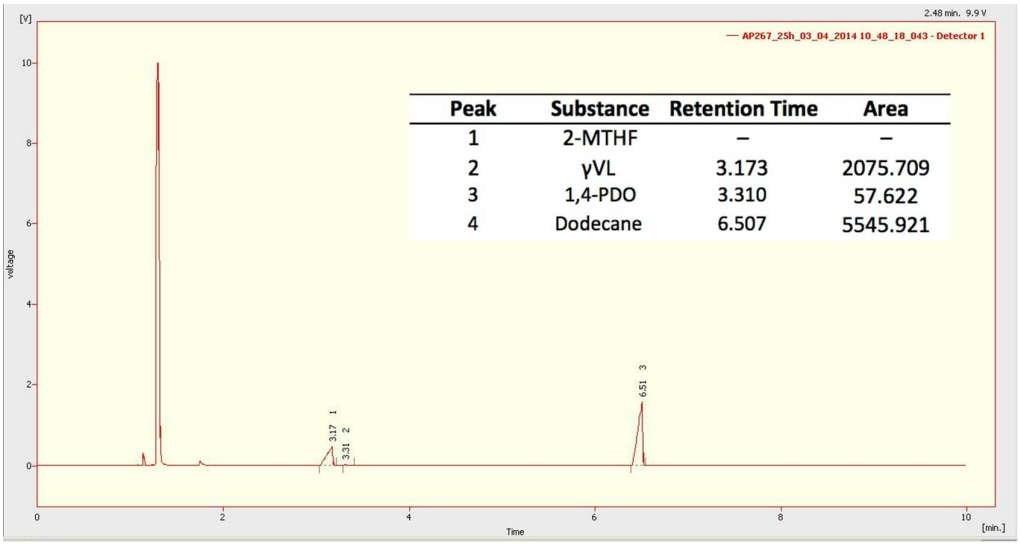

Peak	Substance	Retention Time	Area
1	2-MTHF	–	–
2	γVL	3.173	2075.709
3	1,4-PDO	3.310	57.622
4	Dodecane	6.507	5545.921

Figure S8. Gas chromatogram of final reaction mixture after hydrogenation of levulinic acid using [$RuH_2(CO)\{CH_3C(CH_2PPh_2)_3$-$\kappa^3P\}$] (**3**) and NH_4PF_6 as pre-catalyst. The stated areas were corrected using K_F values determined by calibration experiments with pure substance mixtures.

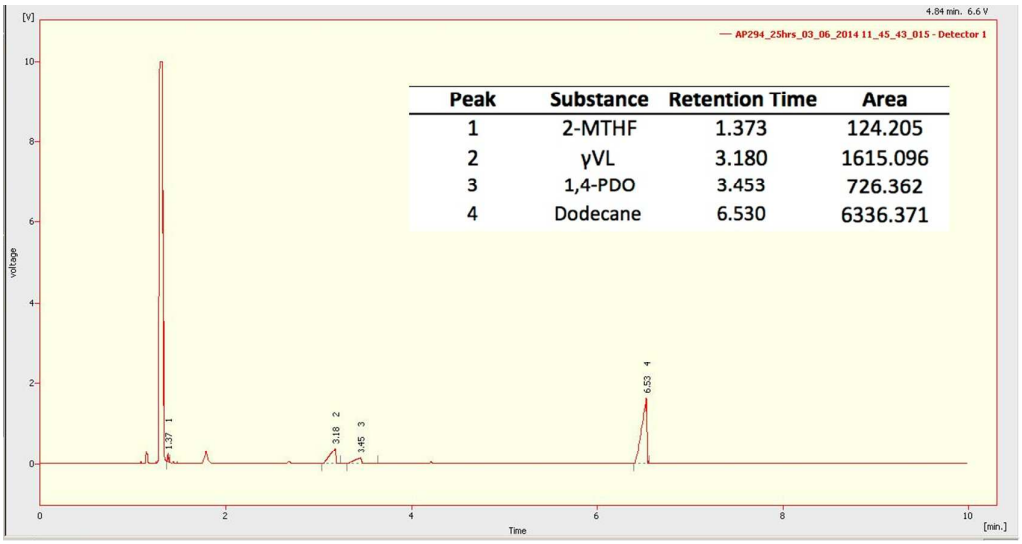

Peak	Substance	Retention Time	Area
1	2-MTHF	1.373	124.205
2	γVL	3.180	1615.096
3	1,4-PDO	3.453	726.362
4	Dodecane	6.530	6336.371

Figure S9. Gas chromatogram of final reaction mixture after hydrogenation of levulinic acid using N-triphos^{Ph}/[Ru(acac)$_3$] and NH_4PF_6 to generate the catalyst *in situ*. The stated areas were corrected using K_F values determined by calibration experiments with pure substance mixtures.

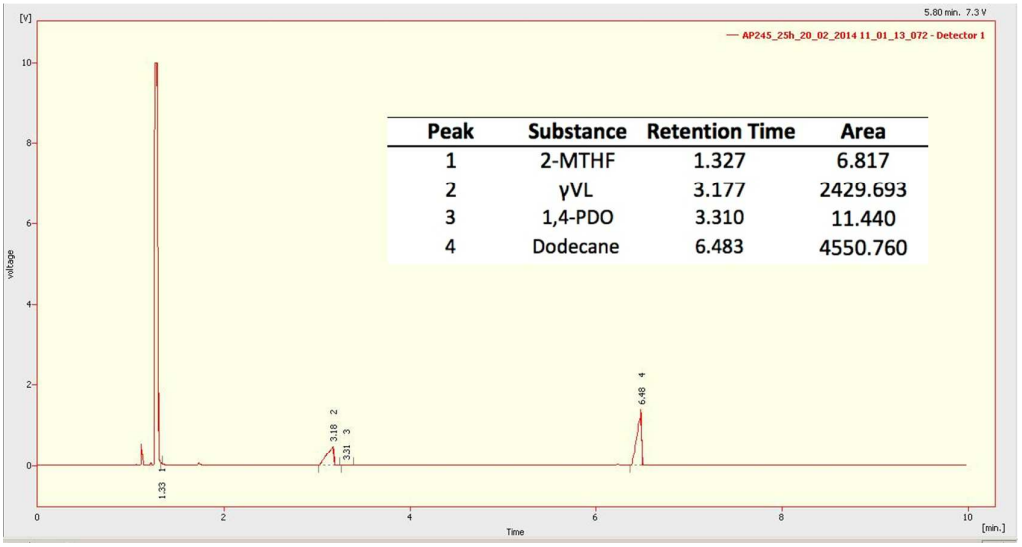

Peak	Substance	Retention Time	Area
1	2-MTHF	1.327	6.817
2	γVL	3.177	2429.693
3	1,4-PDO	3.310	11.440
4	Dodecane	6.483	4550.760

Figure S10. Gas chromatogram of final reaction mixture after hydrogenation of levulinic acid using $[RuH_2(CO)\{N(CH_2PPh_2)_3\text{-}\kappa^3P\}]$ (**4**) and NH_4PF_6 as pre-catalyst. The stated areas were corrected using K_F values determined by calibration experiments with pure substance mixtures.

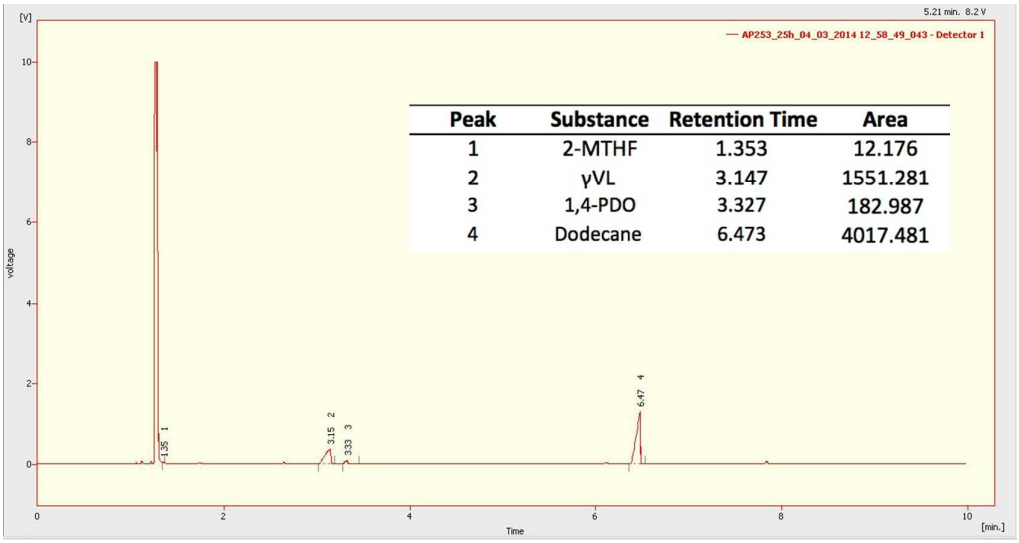

Figure S11. Gas chromatogram of final reaction mixture after hydrogenation of levulinic acid using $[RuH_2(PPh_3)\{N(CH_2PPh_2)_3\text{-}\kappa^3P\}]$ (**5**) and NH_4PF_6 as pre-catalyst. The stated areas were corrected using K_F values determined by calibration experiments with pure substance mixtures.

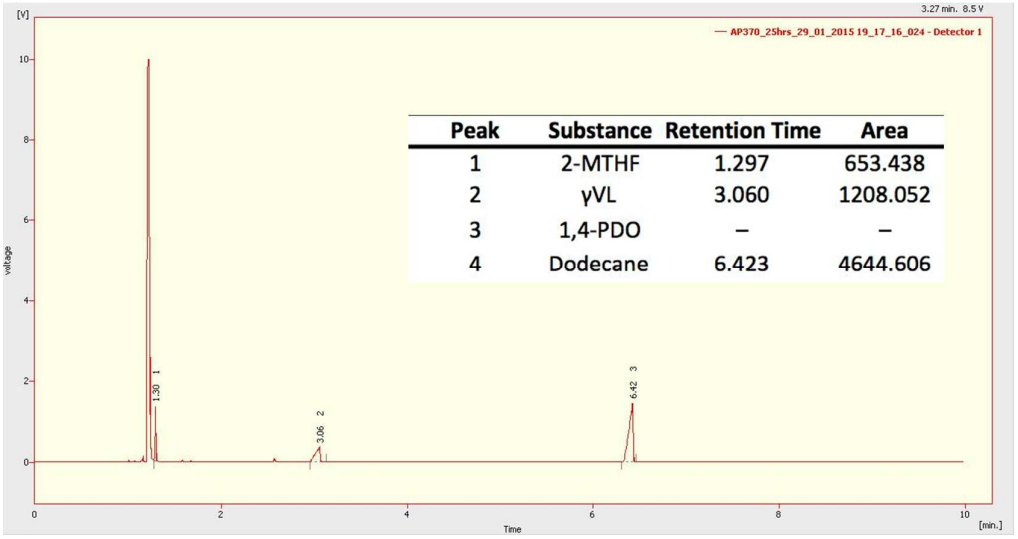

Figure S12. Gas chromatogram of final reaction mixture after hydrogenation of levulinic acid using N-triphos^{Ph}/$[Ru(acac)_3]$ and $HN(Tf)_2$ to generate the catalyst *in situ*. The. The stated areas were corrected using K_F values determined by calibration experiments with pure substance mixtures.

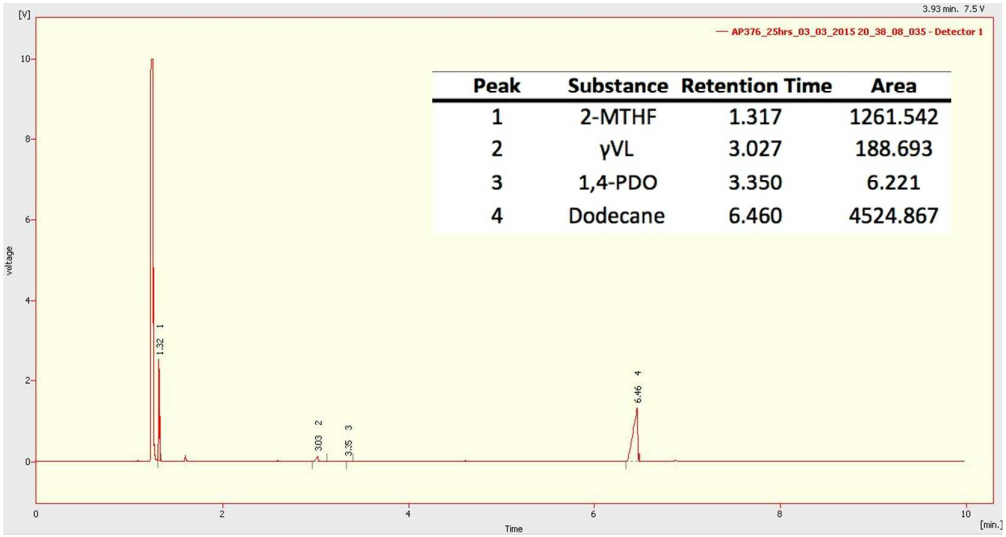

Figure S13. Gas chromatogram of final reaction mixture after hydrogenation of levulinic acid using $[RuH_2(PPh_3)\{N(CH_2PPh_2)_3\text{-}\kappa^3P\}]$ (**5**) and $HN(Tf)_2$ to generate the catalyst *in situ*. The stated areas were corrected using K_F values determined by calibration experiments with pure substance mixtures.

Mercury poisoning experiment

Table S1. Conversion of levulinic acid and yields of products after mercury poisoning of catalytic system and control reaction without mercury poisoning.[a]

Entry	Catalyst	Time [h]	Conversion [%]	Yield [%] γVL	1,4-PDO	2-MTHF
1[b]	N-triphos^{Ph}/[Ru(acac)$_3$]	2	42	41	0	0
2[b]	N-triphos^{Ph}/[Ru(acac)$_3$]	8	77	76	0	0
3	N-triphos^{Ph}/[Ru(acac)$_3$]	2	42	41	0	0
4	N-triphos^{Ph}/[Ru(acac)$_3$]	8	73	70	0	0

[a]Conditions: 10 mmol LA, 20 mL THF, 0.5 mol % [Ru(acac)$_3$], 1.0 mol % N-triphos^{Ph}, 150 °C, 8 h. [b]Depressurized and elemental mercury added to reaction solution after 2 h and stirred at room temperature for 2 h before separation and re-subjecting to catalytic conditions (see Experimental for complete details).

Additional catalytic data

Table S2. Additional catalytic data varying amount of acidic additive, pressure and solvent.[a]

Entry	Catalyst	Additive (mol %)	Pressure	Yield [%] γVL	1,4-PDO	2-MTHF
1	**4**	NH_4PF_6 (5 mol %)	65	95	<1	0
2	**4**	NH_4PF_6 (1 mol %)	65	98	<1	1
3	**4**	NH_4PF_6 (10 mol %)	65	79	8	1
4	**4**	NH_4PF_6 (5 mol %)	95	84	1	<1
5[b]	**4**	NH_4PF_6 (5 mol %)	65	68	<1	0

[a]Conditions: 10 mmol LA, 20 mL THF, 0.5 mol % **4**, 150 °C, 25 h. [b]Dioxane solvent. Full conversion was achieved in all cases.

$^{31}P\{^{1}H\}$ NMR spectra of complexes 8 and 10

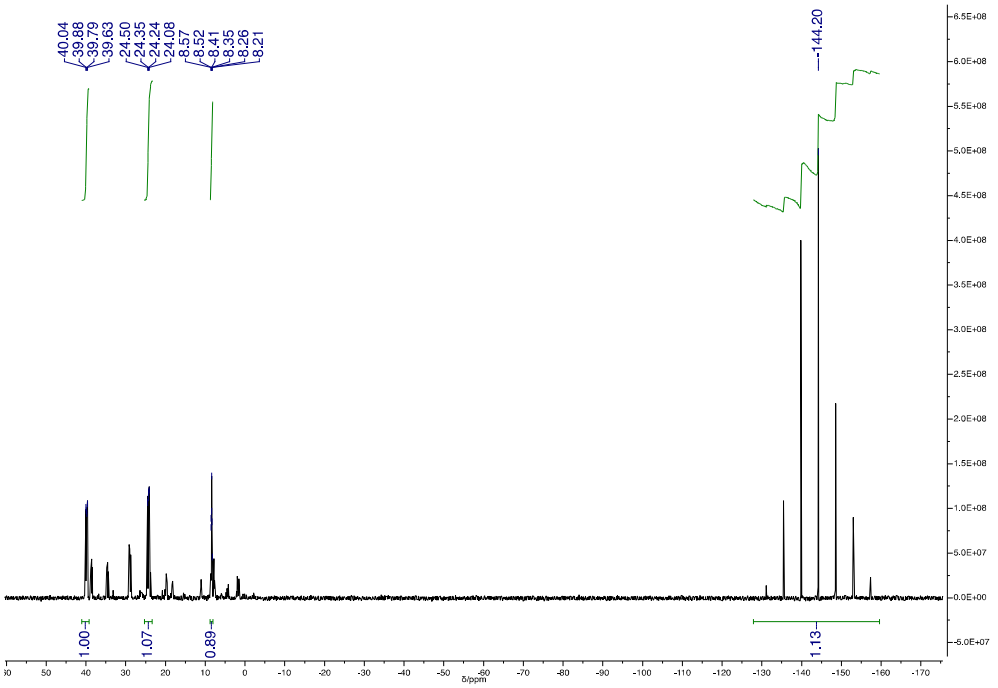

Figure S14. Impure $^{31}P\{^{1}H\}$ NMR spectrum of $[RuH(CO)(NCMe)\{CH_3C(CH_2PPh_2)_3\text{-}\kappa^3\mathit{P}\}][PF_6]$ (**8**) formed from the NMR-scale reaction of $[RuH_2(CO)\{CH_3C(CH_2PPh_2)_3\text{-}\kappa^3\mathit{P}\}]$ (**3**) with NH_4PF_6.

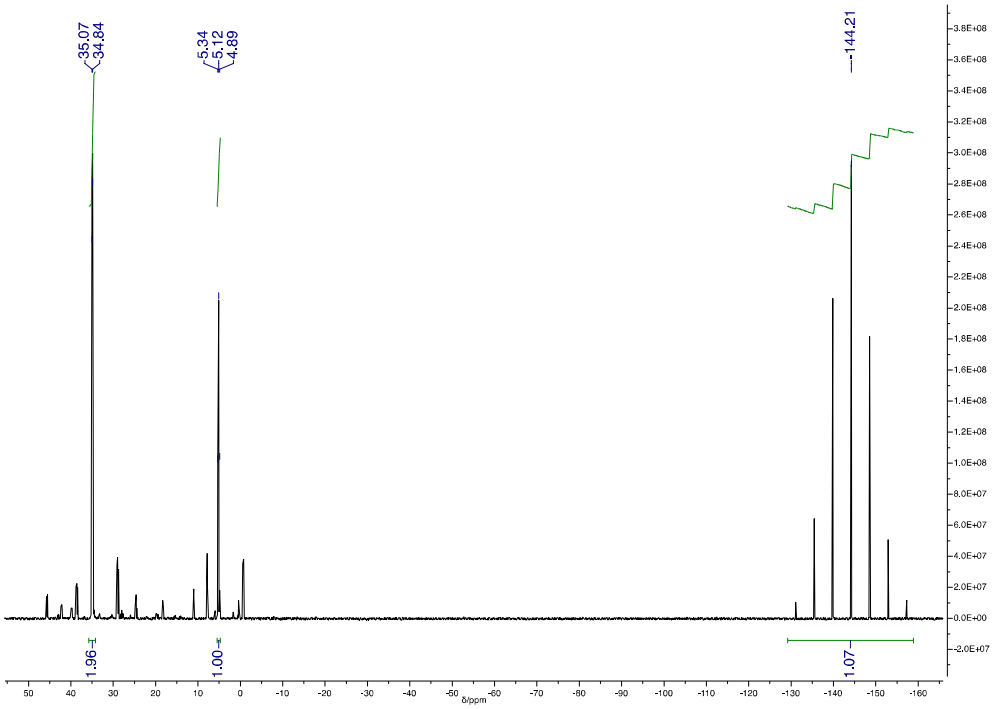

Figure S15. Impure $^{31}P\{^{1}H\}$ NMR spectrum of $[Ru(CO)\{CH_3C(CH_2PPh_2)_3\}\text{-}\kappa^3\mathit{P}\{CH_3C(O)(CH_2)_2C(O)O\text{-}\kappa^2\mathit{O}\}][PF_6]$ (**10**) formed from the reaction of $[RuH(CO)(NCMe)\{CH_3C(CH_2PPh_2)_3\text{-}\kappa^3\mathit{P}\}][PF_6]$ (**8**) with levulinic acid.

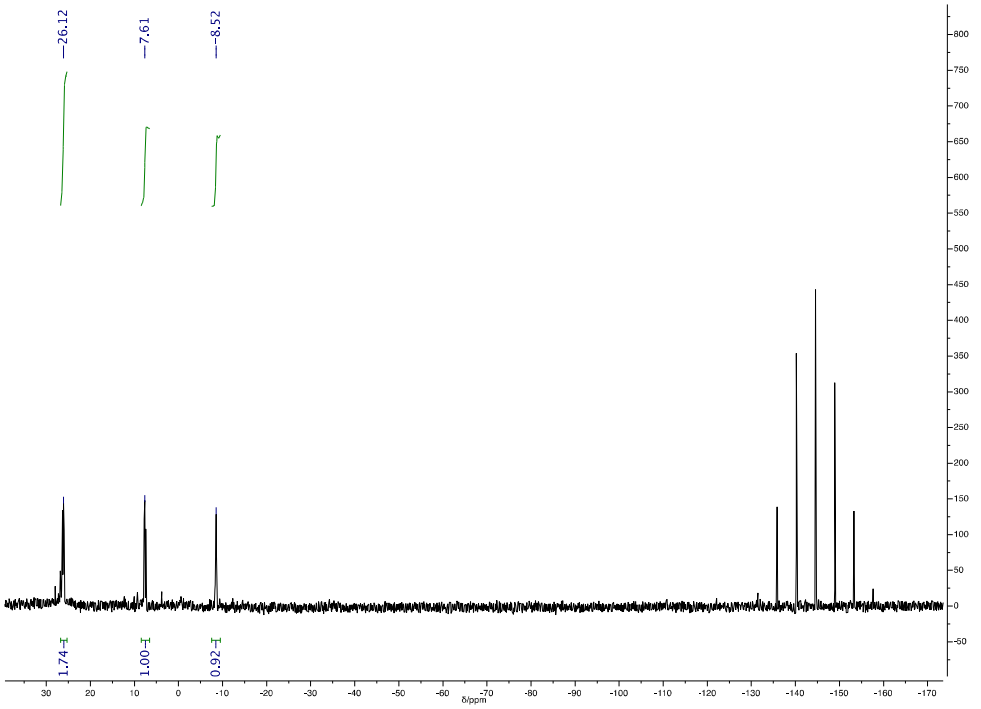

Figure S16. Impure $^{31}P\{^{1}H\}$ NMR spectrum of $[RuH(CO)(NH_3)\{N(CH_2PPh_2)_3\text{-}\kappa^3\mathit{P}\}][PF_6]$ (**13**) formed from the reaction of $[RuH_2(CO)\{N(CH_2PPh_2)_3\text{-}\kappa^3\mathit{P}\}]$ (**4**) with NH_4PF_6 in THF.

^{1}H and $^{31}P\{^{1}H\}$ NMR spectra of complexes 14–16

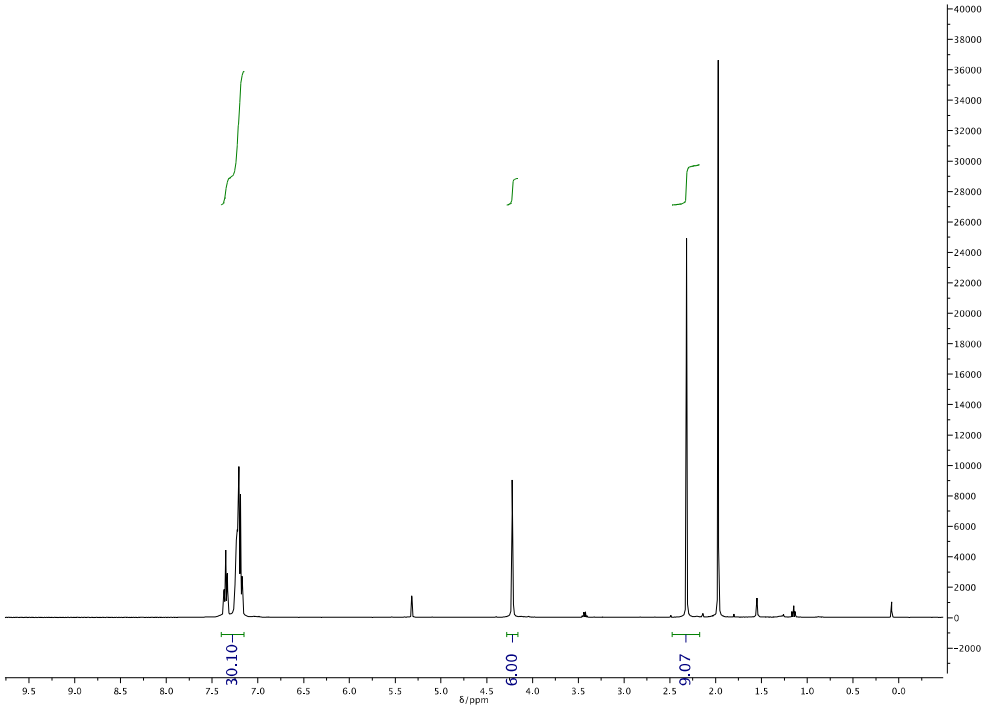

Figure S17. ^{1}H NMR spectrum of $[Ru(NCMe)_3\{N(CH_2PPh_2)_3\text{-}\kappa^3\mathit{P}\}][PF_6]_2$ (**14**).

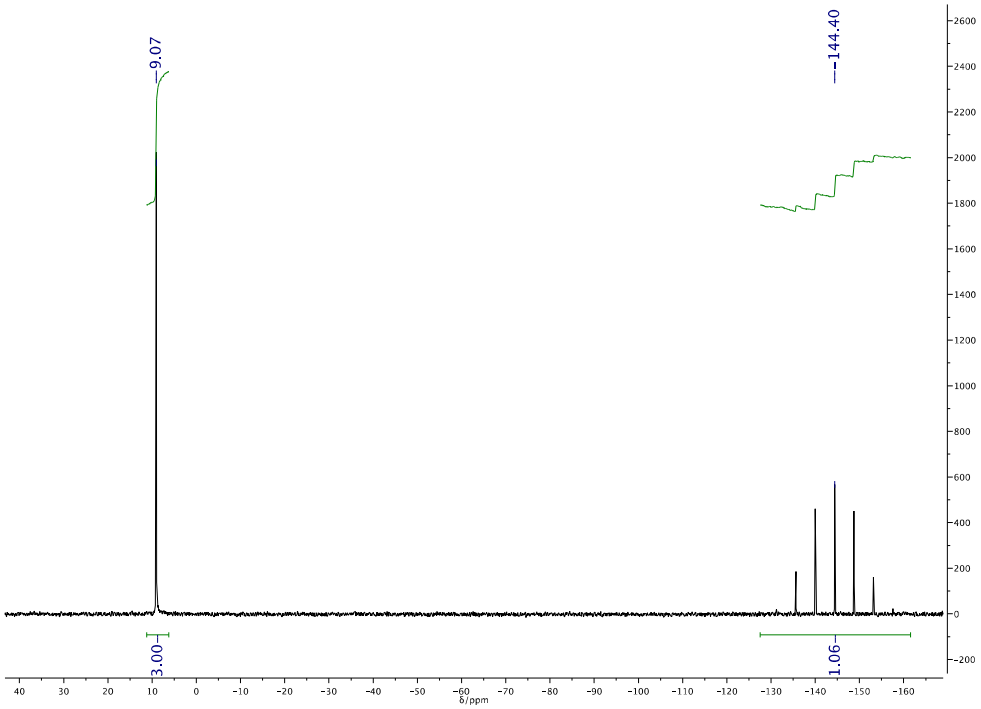

Figure S18. $^{31}P\{1H\}$ NMR spectrum of $[Ru(NCMe)_3\{N(CH_2PPh_2)_3\text{-}\kappa^3P\}][PF_6]_2$ (**14**).

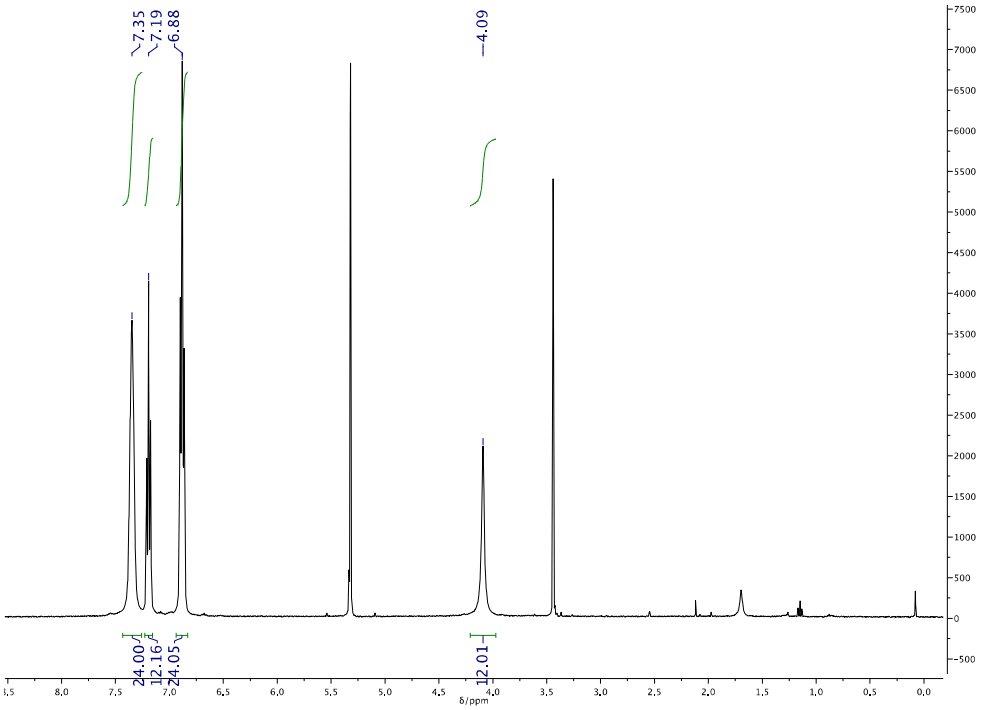

Figure S19. ^{1}H NMR spectrum of $[Ru_2(\mu\text{-}Cl)_3\{N(CH_2PPh_2)_3\text{-}\kappa^3P\}_2][Cl]$ (**15**).

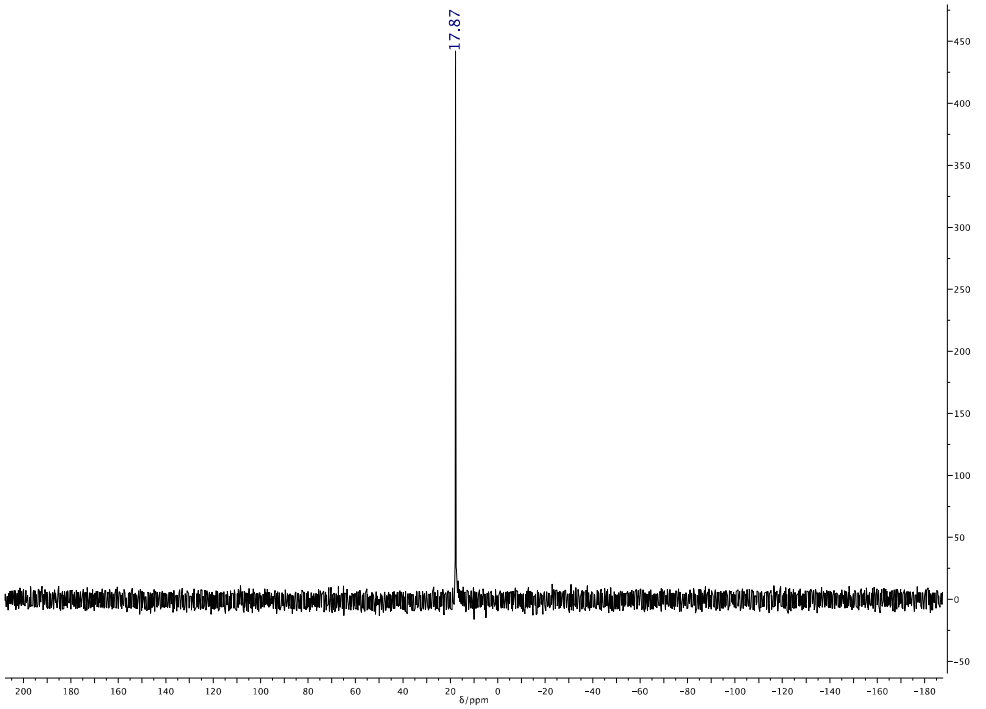

Figure S20. $^{31}P\{^{1}H\}$ NMR spectrum of $[Ru_2(\mu\text{-}Cl)_3\{N(CH_2PPh_2)_3\text{-}\kappa^3P\}_2][Cl]$ (**15**).

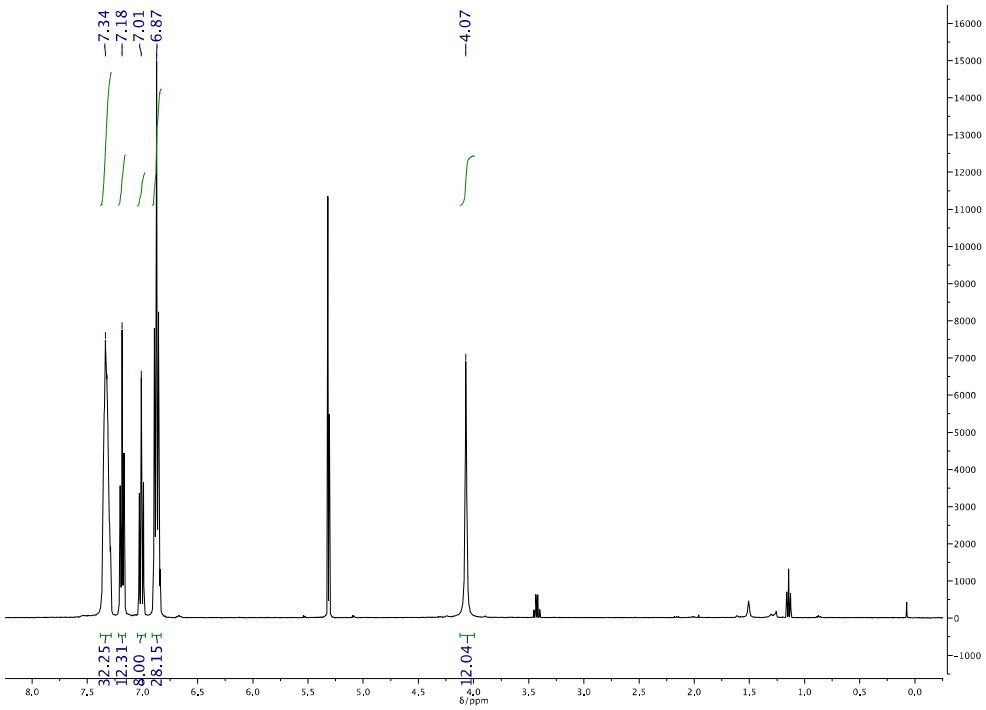

Figure S21. 1H NMR spectrum of $[Ru_2(\mu\text{-}Cl)_3\{N(CH_2PPh_2)_3\text{-}\kappa^3P\}_2][BPh_4]$ (**16**).

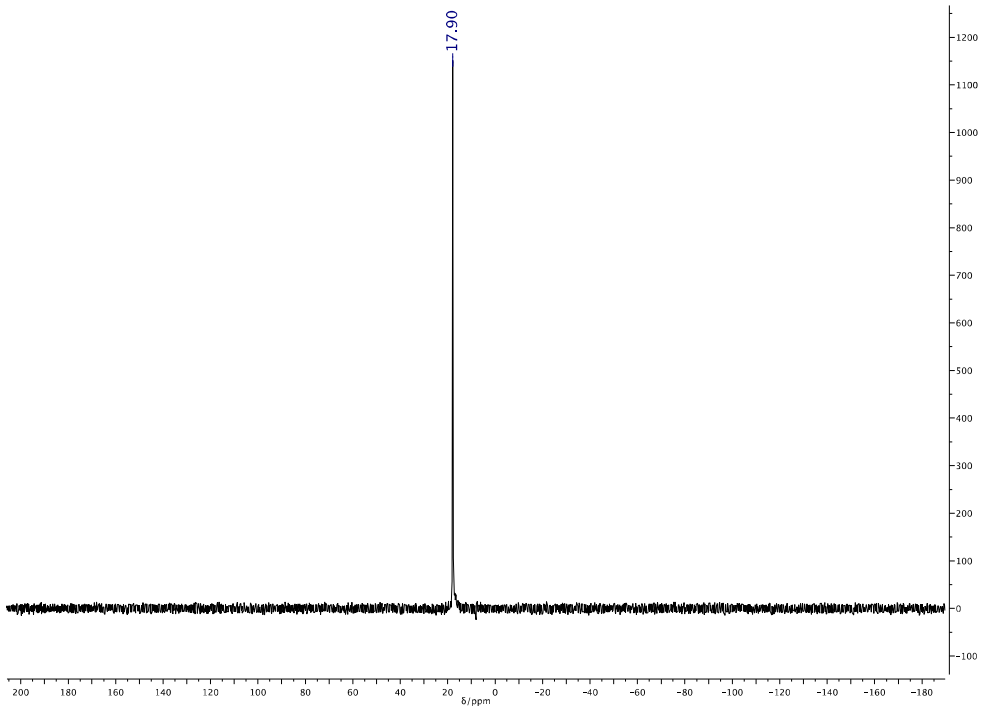

Figure S22. $^{31}P\{^{1}H\}$ NMR spectrum of $[Ru_2(\mu\text{-}Cl)_3\{N(CH_2PPh_2)_3\text{-}\kappa^3P\}_2][BPh_4]$ (**16**).

X-Ray crystallography

X-ray crystal structure of **14**: The crystal structure of **14** was found to contain two independent cations (**14-A** and **14-B**) in the asymmetric unit (see Figures 5 and S3 respectively). The C(20A)-based phenyl ring and the P(20)-based hexafluorophosphate anion were both found to be disordered, and in each case two orientations were identified, of *ca*. 73:27 and 78:22% occupancy respectively. For each pair of orientations the geometries were optimised, the thermal parameters of adjacent atoms were restrained to be similar, and only the non-hydrogen atoms of the major occupancy orientations were refined anisotropically (those of the minor occupancy orientations were refined isotropically).

The included solvent was found to be highly disordered, and the best approach to handling this diffuse electron density was found to be the SQUEEZE routine of PLATON.[X1] This suggested a total of 197 electrons per unit cell, equivalent to 49.3 electrons per complex. The crystal was grown from a mixture of diethyl ether ($C_4H_{10}O$, 42 electrons), acetonitrile (C_2H_3N, 22 electrons), methanol (CH_4O, 18 electrons), dichloromethane (CH_2Cl_2, 42 electrons) and toluene (C_7H_8, 50 electrons), and before the use of SQUEEZE the solvent most resembled acetonitrile. 2.25 acetonitrile molecules corresponds to 49.5 electrons, so this was used as the solvent present. As a result, the atom list for the asymmetric is low by 2 x $2.25(C_2H_3N) = C_9H_{13.5}N_{4.5}$ (and that for the unit cell low by $C_{18}H_{27}N_9$) compared to what is actually presumed to be present.

Crystal data for **14**: $[C_{45}H_{45}N_4P_3Ru](PF6)_2\cdot 2.25MeCN$, $M = 1218.14$, triclinic, P-1 (no. 2), $a = 12.9272(4)$, $b = 20.8705(6)$, $c = 21.4381(6)$ Å, $\alpha = 76.703(3)$, $\beta = 88.780(2)$, $\gamma = 82.119(2)°$, $V = 5575.4(3)$ Å^3, $Z = 4$ (two independent molecules), $D_c = 1.451$ g cm^{-3}, μ(Mo-Kα) = 0.505 mm^{-1}, $T = 173$ K, colourless tabular needles, Agilent Xcalibur 3E diffractometer; 22027 independent measured reflections ($R_{int} = 0.0264$), F^2 refinement,[X1] R_1(obs) = 0.0541, wR_2(all) = 0.1633, 16208 independent observed absorption-corrected reflections [$|F_o| > 4\sigma(|F_o|)$, $2\theta_{max} = 57°$], 1244 parameters. CCDC 1038458.

X-ray crystal structure of **16**: The C(130)-based included dichloromethane solvent molecule in the structure of **16** was found to be disordered. Two orientations were identified

of *ca*. 83 and 17% occupancy, their geometries were optimised, the thermal parameters of adjacent atoms were restrained to be similar, and only the non-hydrogen atoms of the major occupancy orientation were refined anisotropically (those of the minor occupancy orientation were refined isotropically).

Crystal data for **16**: $[C_{78}H_{72}Cl_3N_2P_6Ru_2](C_{24}H_{20}B)\cdot 2CH_2Cl_2$, $M = 2020.74$, orthorhombic, *Pbca* (no. 61), $a = 25.3078(6)$, $b = 26.2242(10)$, $c = 28.1953(7)$ Å, $V = 18712.6(10)$ Å^3, $Z = 8$, $D_c = 1.435$ g cm^{-3}, μ(Mo-Kα) = 0.675 mm^{-1}, $T = 173$ K, yellow tablets, Oxford Diffraction Xcalibur 3 diffractometer; 24856 independent measured reflections ($R_{int} = 0.0310$), F^2 refinement, R_1(obs) = 0.0435, wR_2(all) = 0.1080, 17333 independent observed absorption-corrected reflections [$|F_o| > 4\sigma(|F_o|)$, $2\theta_{max} = 61°$], 1113 parameters. CCDC 1038459.

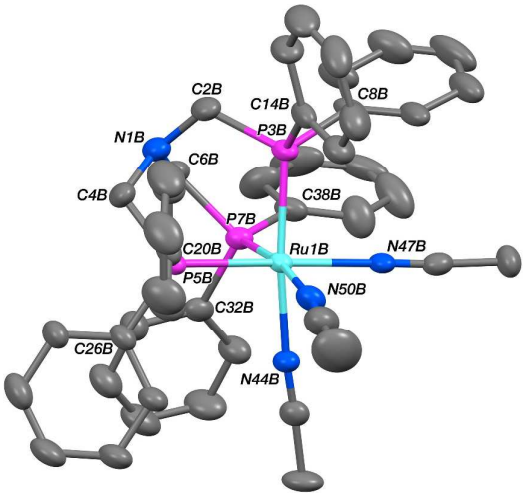

Figure S23. The structure of one (**14-B**) of the two independent cations present in the crystal of **14** (50% probability ellipsoids).

Preliminary density functional theory calculations to demonstrate nitrogen–metal interaction

Density Functional Theory (DFT) studies to obtain further insight into the interaction between the nitrogen and metal center upon coordination of N-triphos^{Ph} (**2**) are currently underway. DFT optimization and frequency analysis calculations were carried out at the B3LYP level of theory for $[RuH_2(CO)\{CH_3C(CH_2PPh_2)_3\text{-}\kappa^3P\}]$ (**3**) and $[RuH_2(CO)\{N(CH_2PH_2)_3\text{-}\kappa^3P\}]$ (**4**) with 6-31g* basis set for all atoms except for ruthenium, for which the Stuttgart-Dresden pseudopotential was used (MWB60). The structures were energy minimized until all the optimization criteria were reached in Gaussian09, and frequency analysis confirmed a true energy minimum structure was obtained from the absence of imaginary frequencies.

Initial results show a N–Ru interaction does exist in **4**, as evident from the contour map of the HOMO (Figure S24A), which shows favourable overlap of nitrogen and ruthenium based orbitals, that appear to originate from atomic orbitals of p and d_{z^2} parentage, respectively. On the other hand, no such evidence is observed for a similar C–Ru interaction in **3**. The calculated contour map of the HOMO of complex **3** (Figure S23B) appears to be purely metal-based and of d_{xy} parentage. Further calculations are currently underway to quantify and expand on this interaction.

A

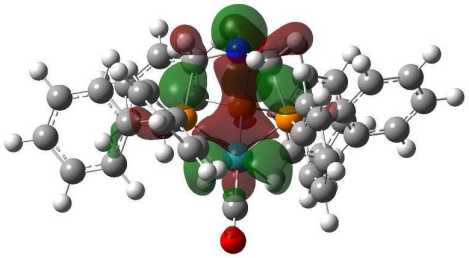

B

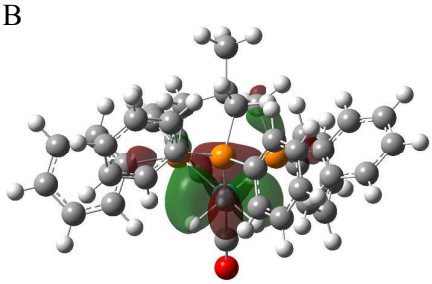

Figure S24. Calculated contour map of HOMOs of **4** (A) and **3** (B) at B3LYP/6-31g*/MWB60 level of theory.

References

[X1] (a) SHELXTL, Bruker AXS, Madison, WI; (b) SHELX-97, G.M. Sheldrick, *Acta Cryst.*, **2008**, *A64*, 112-122; (c) SHELX-2013, http://shelx.uni-ac.gwdg.de/SHELX/index.php